Mon. Not. R. astr. Soc. (1991) **249**, 596–601

Vlasov–Maxwell equilibria of solar coronal loops

V. Krishan and T. D. Sreedharan
Indian Institute of Astrophysics, Bangalore 560034, India

Swadesh M. Mahajan
Institute for Fusion Studies, The University of Texas at Austin, Austin, Texas 78712, USA

Accepted 1990 October 29. Received 1990 October 9; in original form 1990 July 2

SUMMARY

A Vlasov–Maxwell description of the ubiquitous solar coronal structures is presented. It is found that an equilibrium plasma configuration can live with spatial gradients in density, temperature, current and drift speeds of the charged particles. Any stability study must be carried over this inhomogeneous equilibrium state. In addition, the Vlasov description admits the investigation of kinetic processes like heating and radiation and unlike a fluid description, it does not require an equation of state to determine the individual variations of temperature and density.

1 INTRODUCTION

Solar coronal loops have been studied conventionally through magnetohydrodynamic processes, since their shapes betray the underlying magnetic fields. Coronal loops are especially favoured for their ability to pick up energy from the convection zone and deposit it in the corona. The foot points of the loops suffer continuous turning and twisting, producing complex magnetic geometry in which current sheets have been shown to form. One believes that ohmic dissipation of current in these sheets can maintain a $\sim 10^6$ K corona. Attempts to show the formation of extremely small-scale current sheets have been carried out by Parker (1983, 1987), Low (1987), Low & Wolfson (1988), Van Ballegooijen (1985, 1986), Karpen, Antiochos & De Vove (1990) and many more. The MHD equilibria of coronal loops have been investigated by Priest (1981), Hood & Priest (1979), Vaiana & Rosner (1978), Tsinganos (1982), Krishan (1983, 1985) and Krishan, Berger & Priest (1988). In this paper, we explore a Vlasov–Maxwell treatment of a current-carrying cylindrical plasma. In this description, it is possible to derive the spatial profiles of equilibrium plasma parameters and the exact particle velocity distributions without invoking equations of state and the exact particle velocity distribution functions. It is found that the system develops strongly-peaked current density profiles under very commonly occurring conditions. It is perhaps the disturbance of these current density configurations that leads to the heating and acceleration of particles in coronal loops.

2 VLASOV–MAXWELL EQUILIBRIA

We will closely follow the recent work of Mahajan (1989) on Vlasov–Maxwell equilibria for several systems, the exemplary cases being Z pinches and Tokamaks. A coronal loop will be represented by a cylindrical column of plasma with current density J_Z along the axis of the cylinder and with no gravity. The actual geometry of a coronal loop consists of the two ends (the foot prints) of the cylindrical plasma embedded in a sub-photospheric region. A small twisting motion of the foot points may introduce a small amount of azimuthal current J_θ which we neglect at present. The sub-photospheric region contains a high-β plasma where β is the ratio of gas kinetic pressure to magnetic pressure. As a result the magnetic field lines move on a time-scale much longer than the coronal time-scales. This line tying reduces the region of unstable excitations, especially those of long wavelength. The neglect of gravity reduces the coronal loop to an essentially horizontal cylinder. Of course, while studying the stability of an equilibrium, the end effects, gravity and curvature must be properly taken into account. The particle density n, the temperature T, and the particle drift speeds u are in general, spatially varying quantities. Here we allow all spatial variations only in the radial direction since there is observational evidence for such variations. The plasma is embedded in a uniform axial magnetic field, B_0. The relevant equations for an equilibrium system (with $\partial/\partial t = 0$) are

$$V_r \frac{\partial f_e}{\partial r} - \frac{e}{m_e}\left[\boldsymbol{E} + \frac{\boldsymbol{V}}{c} \times (\boldsymbol{B} + \hat{e}_z B_0)\right] \cdot \frac{\partial f_e}{\partial \boldsymbol{V}} = 0 \tag{1}$$

$$V_r \frac{\partial f_i}{\partial r} + \frac{e}{m_i}\left[\boldsymbol{E} + \frac{\boldsymbol{V}}{c} \times (\boldsymbol{B} + \hat{e}_z B_0)\right] \cdot \frac{\partial f_i}{\partial \boldsymbol{V}} = 0 \tag{2}$$

$$\frac{1}{r}\frac{\partial}{\partial r}(rB_\theta) = \frac{4\pi}{c} J_z \tag{3}$$

$$\nabla \cdot \boldsymbol{E} = 0 \tag{4}$$

$$\nabla \times \boldsymbol{E} = 0 \tag{5}$$

$$J_z = -e \int d^3V v_z (f_e - f_i) \tag{6}$$

where $f_{i,e}$ are the single particle distribution functions, ($\boldsymbol{E}$, $\boldsymbol{B}$) are the self consistent fields. Equations (1) and (2) are collisionless Boltzman equations for electrons and ions describing the conservation of particles in phase space of positions and momenta. These are also known as Vlasov equations which are valid at high temperatures when Coulomb collisions can be neglected. In addition the fully ionized plasma considered here experiences only electromagnetic forces. All non-electromagnetic forces, such as gravity, are neglected. Further, the axial dependence of particle density is neglected. This is valid for loops of length smaller than the density scale height. Equation (3) is the axial component of Ampere's law describing steady state fields. Equation (4) is Poisson's equation under the condition of zero charge separation which is justified for an equilibrium study since charge separation occurs over extremely short time-scales such as those of electron plasma oscillation. Equation (5) is Faraday's Law for steady fields. Equation (6) defines current in terms of the particle distribution function for electrons and ions. Let a displaced Maxwellian of the form

$$f_{e,i} = \frac{n_0}{\pi^{3/2} v_{e,i}^3} \exp[-(V - u_z^{e,i})^2 / v_{e,i}^2] g(r) \tag{7}$$

provide a self-consistent solution for equations (1)–(6). Here n_0 is the ambient density, $v_{e,i}^2 = 2T_{e,i}/m_{e,i}$ and $u_z^{e,i}$ are, respectively, the thermal speed and the drift speed, $T_{e,i}$ and $m_{e,i}$ are the temperature and mass and $g(r)$ is the density profile factor which is same for electrons and ions under the assumption of no charge separation.

Case I

The self-consistent solutions of equations (1)–(7) for the case when $g(r)$, describing the entire spatial variation are found to be

$$g(r) = [1 + r^2/4\delta_e^2]^{-2} \tag{8}$$

and

$$b\delta_e = -\left(\frac{r}{\delta_e}\right)[1 + r^2/4\delta_e^2]^{-1} \tag{9}$$

where

$$b = \frac{e u_z^e B_\theta}{C T_e}; \quad \delta_e^2 = \frac{2c^2}{\omega_{pe}^2} \frac{V_e^2 (1-\mu)^{-1}}{2(u_z^e)^2} \tag{10}$$

and

$$\mu = (u_z^i / u_z^e)$$

Here e is the charge, c is the speed of light and $\omega_{pe} = (4\pi n e^2/m_e)^{1/2}$ is the electron plasma frequency. Thus one obtains a density profile peaked at the axis with a characteristic length scale δ_e which will be estimated in a later section.

Case II

Here, in addition to density gradient, the spatial variation of temperature is also allowed. The drift speeds $u_z^{e,i}$ are still homogeneous. It has been shown (Mahajan 1989) that a series representation for the distribution functions gives a valid solution of the inhomogeneous Vlasov–Maxwell system, the expansion parameter for the series being (u/v), the ratio of drift and thermal speeds. This is appropriate for the considerations in coronal loops as discussed later. Using the smallness of (u/v), we write for the distribution function as

$$f_{e,i} = \frac{n_0 g(r)}{\pi^{3/2} (v_0^{e,i} \psi_{e,i})^3} \exp\left[-\frac{v^2}{(v_0^{e,i}\psi_{e,i})^2}\right] \times \left[1 + \frac{2u_z^{e,i}}{v_0^{e,i}} \sum_{n=1}^{\infty} \sum_{m=0}^{\infty} c_{nm} \left(\frac{v_z}{v_0^{e,i}}\right)^n \left(\frac{v}{v_0^{e,i}\psi_{e,i}}\right)^{2m}\right] \tag{11}$$

where ψ_e describes the spatial variation of electron temperature and v_0^e is the thermal speed on the axis ($r = 0$). Since we are interested in equilibrium solutions, we assume $\psi_e = \psi_i = \psi$ and $\beta_e = \beta_i$, i.e. the electrons and ions have identical temperature profiles. With the assumption that density variation is generally steeper than temperature variation, one can take $\beta_e = \beta_i = -\beta$, where $C_{10} = 1$ and $C_{11} = \beta$.

Using equation (11), and retaining terms only up to (u/v), one finds the profile functions as

$$\psi = (1 + r^2/4\delta_{eff}^2)^{-2\beta/5\beta - 2} \tag{12}$$

$$g = (1 + r^2/4\delta_{eff}^2)^{-2(3\beta-2)/5\beta - 2} \tag{13}$$

$$b\delta_{eff} = \left(\frac{5\beta}{2} - 1\right)^{-1} \frac{(r/\delta_{eff})}{(1 + r^2/4\delta_{eff}^2)} \tag{14}$$

where

$$\delta_{eff} = (2\delta_e/5\beta - 2).$$

The temperature

$$T \propto \psi^2 = (1 + r^2/4\delta_{eff}^2)^{-4\beta/5\beta - 2} \tag{15}$$

The current density

$$J_z \propto g\psi^2 = (1 + r^2/4\delta_{eff}^2)^{-2} \tag{16}$$

The pressure

$$p \propto g\psi^2 = (1 + r^2/4\delta_{eff}^2)^{-2} \tag{17}$$

One observes that, depending upon the value of β, the radial variation can be positive or negative. Thus for $\beta > \frac{2}{3}$, both density and temperature fall away from the axis, whereas for $\frac{2}{3} > \beta > \frac{2}{5}$, the density increases and temperature decreases away from the axis. For $\beta < \frac{2}{5}$ the temperature increases towards the surface and this is very much reminiscent of the cool-core- and hot-sheath-type loops observed by Foukal (1978) and Krieger, de Feiter & Vaiana (1976), and modelled through variational principle in MHD by Krishan (1983, 1985). The other parameter, δ_e, which characterizes the spatial variations, is related to the skin depth. We shall see in a later section that the measure of δ_e, which determines the steepness and extent of the current density profile is commensurate with the requirements laid down by the joule heating of the loop plasma.

Case III

Here, we allow gradients in density and drift speed. It is found that the presence of temperature anisotropy permits a

displaced Maxwellian solution of the system where the distribution functions are given by

$$f_{e,i}=\frac{n_0 g(r)}{\pi^{3/2} v_{e,i}^2 v_z^{e,i}} \exp\left\{-\frac{v_r^2+v_\theta^2}{v_{e,i}^2}-\frac{[v_z-u_{0z}^{e,i}\phi_{e,i}(r)]^2}{(v_z^{e,i})^2}\right\} \tag{18}$$

Here, we have taken $\phi_e=\phi_i=\phi$ with $\phi(r=0)=1$, and $g(r=0)=1$. The equations relating the density profile, $g(r)$, and the drift speed profile, ϕ, are found to be

$$\frac{1}{r}\frac{\partial}{\partial r}\left(r\frac{\partial\phi}{\partial r}\right)=-\frac{2\lambda}{\delta_e^2}\exp\left[\left(\frac{u_{0z}^e}{v_z^e}\right)^2(\phi^2-1)\right] \tag{19}$$

and

$$g(r)=\exp\left[\left(\frac{u_{0z}^e}{v_z^e}\right)^2(\phi^2-1)\right] \tag{20}$$

where

$$\lambda=(v_e^2-v_z^2)/2(u_{0z}^e)^2=\frac{T_e-T_{ez}}{m_e(u_{0z}^e)^2}=\frac{\Delta T_e}{2T_e}\frac{v_e^2}{(u_{0z}^e)^2} \tag{21}$$

Equation (19) has been solved numerically and here we will reproduce some of the figures from Mahajan (1989), since the spatial behaviour of the density, the magnetic field and the current density are essentially a function of the dimensionless parameter λ.

Coronal loops

Coronal loop, a bipolar structure is characterized by an electron density $n_0 \sim 10^{10}$–10^{12} cm^{-3}; a temperature varying from a few tens of thousands to a couple of million K, a length of 10^9–10^{10} cm and a radius of 10^8–10^9 cm with an axial magnetic fields of a few Gauss. The current flows essentially along the axis of the cylindrical plasma column and produces an azimuthal component B_θ of the magnetic field. Observations in *EUV* has shown that loops of different temperatures are coaxial and this has led to the identification of cool-core and hot-sheath-type loops, (Foukal 1978; Krishan 1983, 1985). The X-ray observations further reinforce the inhomogeneous nature of the underlying heating mechanisms. Resonance absorption of surface MHD waves, as well as the joule dissipation of high-density current sheets (in addition to the ubiquitous mini magnetic reconnections) are some of the favoured candidates for heating of the solar corona in general, and coronal loops in particular (Hollweg 1981). Here we find that the exact solution of a Vlasov–Maxwell system naturally admits the peaked spatial profiles of current density and magnetic field, and we believe it is this equilibrium configuration, which when disturbed, gives rise to sporadic flaring phenomena, acceleration and heating. It has been shown by Rosner *et al.* (1978) and Hollweg (1981) that for the joule dissipation to provide enough heating to balance the radiation losses for the typical conditions of electron density, magnetic field and temperature, the current sheath must have a thickness of a few hundred to a thousand cm, and anomalous instead of the collisional resistivity must be operative. The latter gives us a clue to the relative electron–ion drift velocity that must exist to excite ion–acoustic turbulence which may be responsible for anomalous resistivity. The typical parameters in this scenario are chosen from Hollweg (1981):

electron density in the sheath–$n_0=10^9$ cm^{-3};
electron temperature in the sheath–$T_e=2.5\times10^7$ K;
electron thermal speed–$V_e=2.7\times10^9$ cm s^{-1};
electron drift velocity $u_e>$ sound speed–$=4.5\times10^7$ cm s^{-1};

The magnetic field B_θ produced by the current density J_z is 10 G, and the thickness (ΔR) of the current sheet turns out to be $\sim10^3$ cm. We recall from the previous section that δ_e is the characteristic length-scale in the solutions of the Vlasov–Maxwell system. Let us estimate it:

$$\delta_e=\frac{c}{\omega_{pe}}\frac{V_e}{u_e}(1+\sqrt{T_i/T_e})^{-1/2}$$

$$=1.04\times10^3 \text{ cm for } T_e\gg T_i,$$
$$=0.9\times10^3 \text{ cm for } T_e=9\,T_i.$$

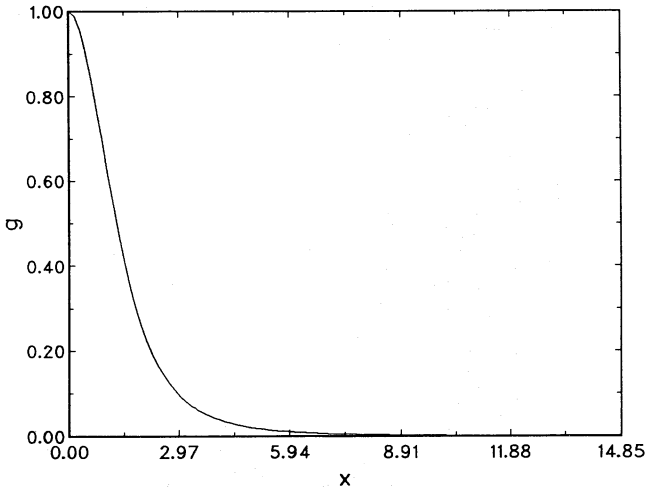

Figure 1. Variation of density profile function $g(r)$ versus $x=r/\delta_e$ for case I (equation 8).

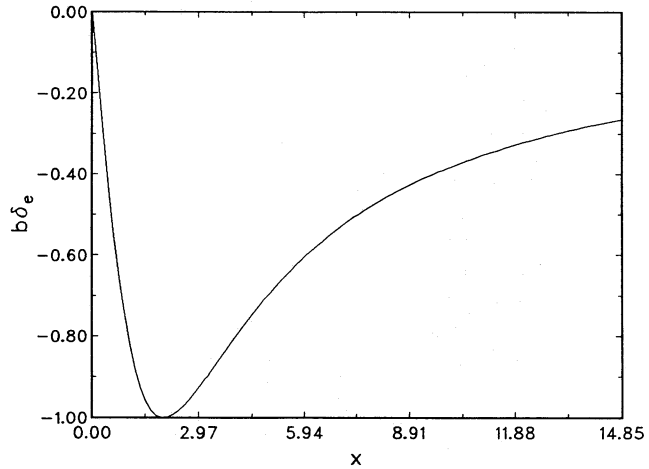

Figure 2. Variation of magnetic-field profile function ($b\ \delta_e$) versus $x=r/\delta_e$ for case I (equation 9).

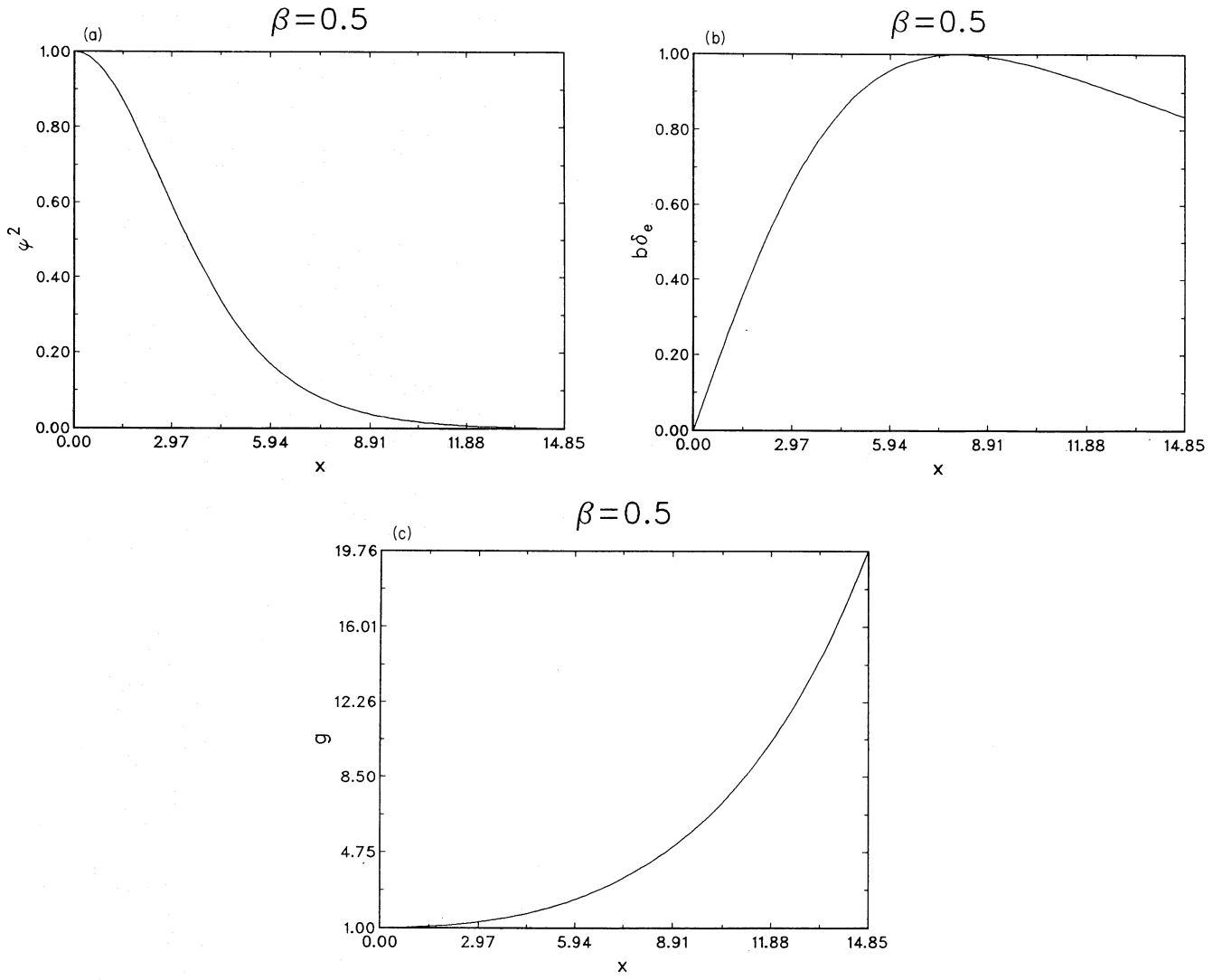

Figure 3. (a) Variation of temperature profile function ψ^2 versus $x = r/\delta_e$ for $\beta = 0.5$ (equation 15). (b) Variation of magnetic-field profile function $(b\delta_e)$ versus $x = r/\delta_e$ for $\beta = 0.5$ (equation 14). (c) Variation of density profile function $g(r)$ versus $x = r/\delta_e$ for $\beta = 0.5$ (equation 13).

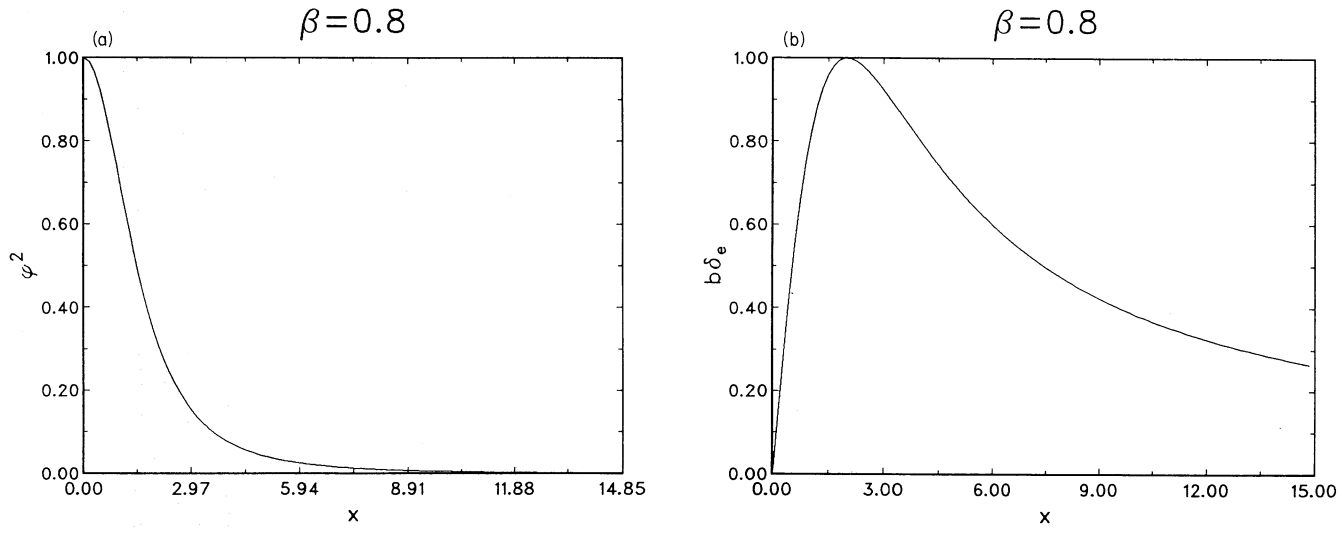

Figure 4. (a) Variation of temperature profile function ψ^2 versus $x = r/\delta_e$ for $\beta = 0.8$. (b) Variation of magnetic-field profile function $(b\delta_e)$ versus $x = r/\delta_e$ for $\beta = 0.8$. (c) Variation of density profile function $g(r)$ versus $x = r/\delta_e$ for $\beta = 0.8$.

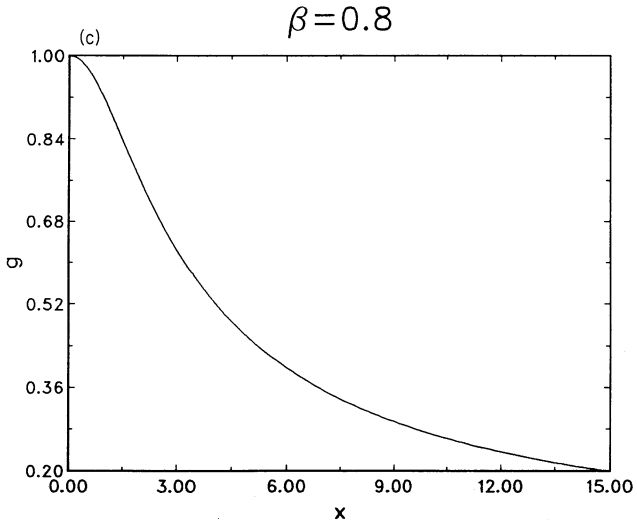

Figure 4 – *continued*

Thus we find that current profile of small widths are the outcome of the exact solutions of the Vlasov–Maxwell system. Here we present a few examples of spatial variations of plasma parameters. The variations of density and magnetic-field profile factors (g and b, respectively) for case I, where only the density is space dependent, are given by equations (8) and (9) and shown in Figs (1) and (2). A sharp fall in density away from the axis is obtained. This is reminiscent of the condensations often observed at the axis of a loop. The current density is therefore found to be maximum on the axis. The spatial profiles for case II allowing temperature variation are given by equations (12), (13) and (14), and are shown in Figs (3), (4) and (5) for three values of the parameter β. In this case the temperature increase (equation 15) away from the axis for $\beta < 2/5$. Case III gives very interesting profiles where the current density appears in the form of multisheaths (Fig. 6) for large values of the anisotropy parameter; the corresponding density profile (Fig. 7) is almost flat. These profiles are reproduced from Mahajan (1989). Since all functions, as well as the variables, are

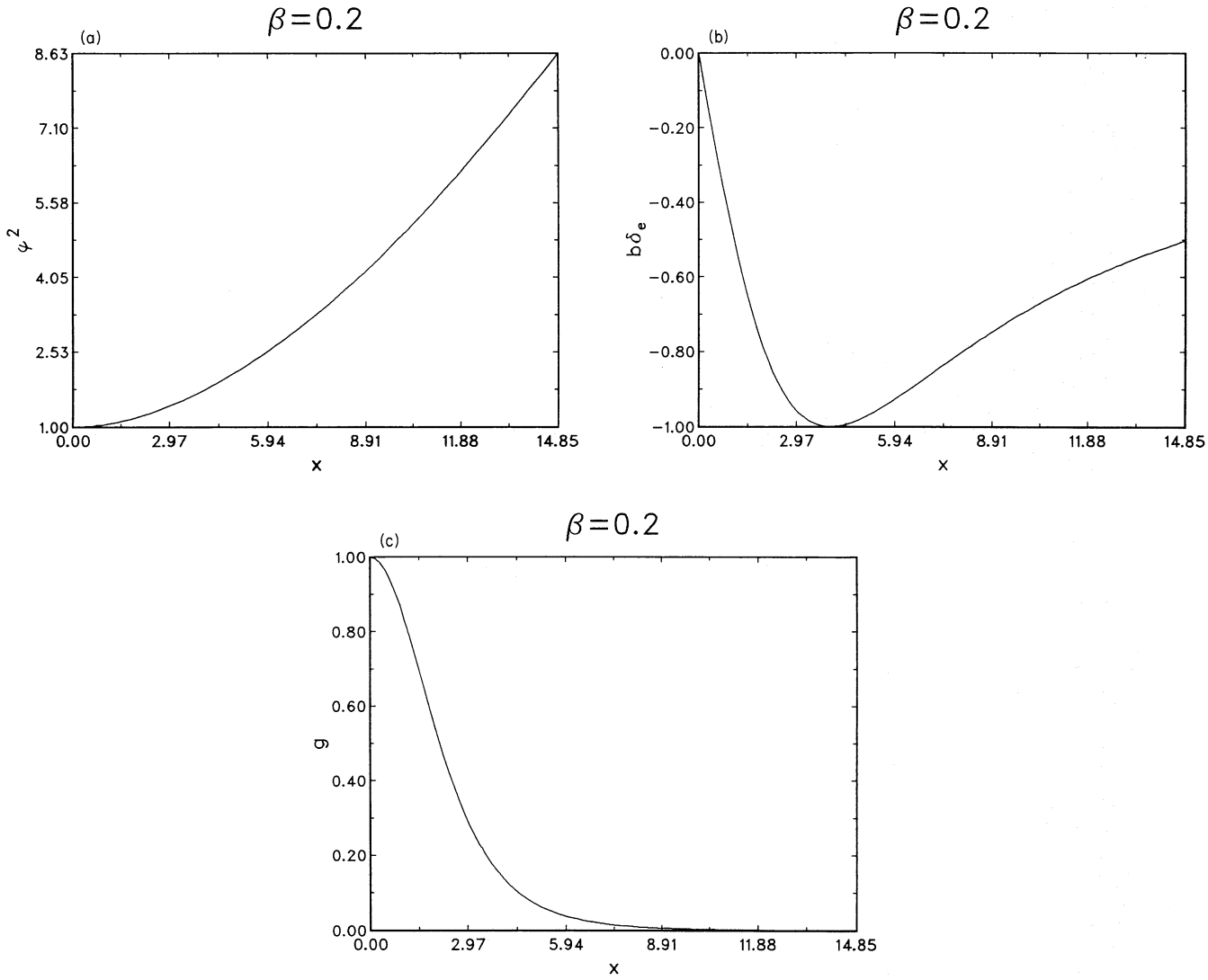

Figure 5. Variation of temperature profile function ψ^2 versus $x = r/\delta_e$ for $\beta = 0.2$. (b) Variation of magnetic-field profile function ($b\delta_e$) versus $x = r/\delta_e$ for $\beta = 0.2$. (c) Variation of density profile function $g(r)$ versus $x = r/\delta_e$ for $\beta = 0.2$.

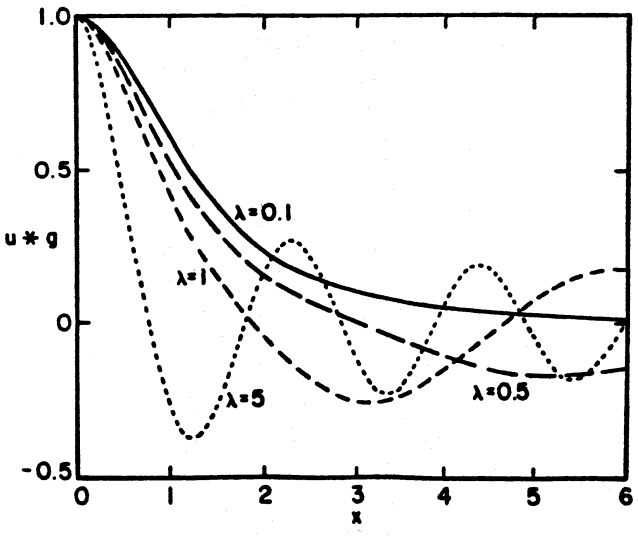

Figure 6. Variation of current profile function (*gue*) versus $x = r/\delta_e$ showing formation of multisheaths for large values of temperature anisotropy parameter λ (from Mahajan 1989).

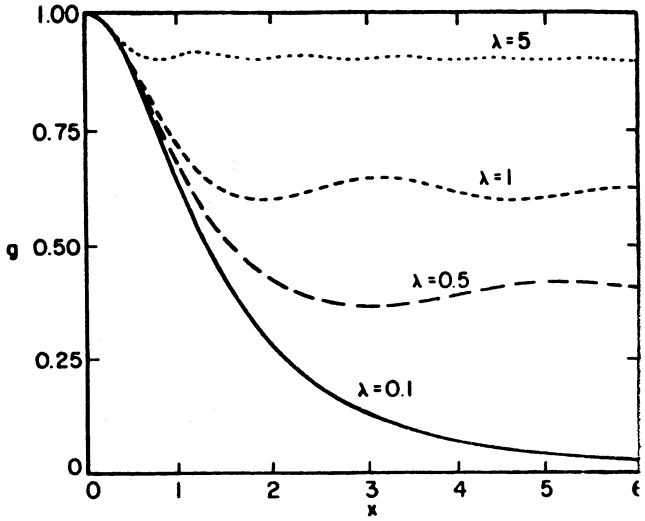

Figure 7. Variation of density profile function $g(r)$ versus $x = r/\delta_e$ for several values of the temperature anisotropy parameter λ (from Mahajan 1989).

expressed in dimensionless forms, we only need to provide appropriate normalization. For coronal loops, the anisotropy parameter

$$\lambda = \frac{\Delta T_e}{T_e}\frac{V_e^2}{2u_e^2} = 1.8 \times 10^3 \frac{\Delta T_e}{T_e}$$

Thus for $\lambda = 5$ one finds $(\Delta T_e/T_e) = 2.7 \times 10^{-3}$, which is reasonably small.

CONCLUSIONS

A Vlasov–Maxwell description of coronal loop plasma admits a variety of equilibrium spatial profiles of mass density, current density, the temperature, and the magnetic field depending upon the type of inhomogeneities allowed. The profiles vary from being flat to spiky and resemble the ones derived from EUV and X-ray coronal observations. The multisheath current profiles derived here complement the magnetohydrodynamic study of current sheet formation especially well. In addition, the Vlasov description allows the determination of density and temperature profiles individually, in contrast to the fluid description where equation of state is required to extract the separate variations of density and temperature from the pressure profile.

REFERENCES

Foukal, P. V., 1978. *Astrophys. J.* **223,** 1046.

Hollweg, J. V., 1981. In: *Solar Active Regions*, p. 277, ed. Orrall, F. Q., Colorado Associated University Press.

Hood, A. W. & Priest, E. R., 1979. *Astr. Astrophys.*, **77,** 233.

Karpen, J. T., Antiochos, S. K. & De Vove, C. R., 1990. *Astrophys. J.*, **356,** L67.

Krieger, A. S., de Feiter, L. D. & Vaiana, G. S., 1976. *Solar Phys.*, **47,** 117.

Krishan, V., 1983. *Solar Phys.*, **88,** 155.

Krishan, V., 1985. *Solar Phys.*, **97,** 183.

Krishan, V., Berger, M. & Priest, E. R., 1988. In: *Solar and Stellar Coronal Structures and Dynamics,* p. 256, ed. Altrock, R. C., National Solar Observatory, Sunspot, New Mexico.

Low, B. C., 1987. *Astrophys. J.*, **323,** 358.

Low, B. C. & Wolfson, R., 1988. *Astrophys. J.*, **324,** 574.

Mahajan, S. M., 1989. *Phys. Fluids B*1, **1,** 43.

Parker, E. N., 1983. *Astrophys. J.*, **264,** 635.

Parker, E. N., 1987. *Astrophys. J.*, **318,** 876.

Priest, E. R., 1981. In: *Solar Flare Magnetohydrodynamics*, p. 2 and 139, ed. Priest, E. R., Gordon and Breach.

Rosner, R., Golub, L., Coppi, B. & Vaiana, G. S., 1978. *Astrophys. J.*, **222,** 317.

Tsinganos, K. C., 1982. *Astrophys. J.*, **259,** 820.

Vaina, G. S. & Rosner, R., 1978. *Ann. Rev. Astr. Astrophys.*, **16,** 393.

Van Ballegooijen, A. A., 1985. *Astrophys. J.*, **298,** 421.

Van Ballegooijen, A. A., 1986. *Astrophys. J.*, **311,** 1001.